Structure determination of micelle-like intermediates in amyloid β-protein fibril assembly by using small angle neutron scattering

Winnie Yong[†‡], Aleksey Lomakin[†], Marina D. Kirkitadze[§], David B. Teplow[§], Sow-Hsin Chen[‡], and George B. Benedek[†¶]

[†]Department of Physics, Center for Materials Science and Engineering, and Materials Processing Center, [‡]Department of Nuclear Engineering, Massachusetts Institute of Technology, Cambridge, MA 02139-4307; and [§]Center for Neurologic Diseases, Brigham and Women's Hospital, and Department of Neurology (Neuroscience), Harvard Medical School, Boston, MA 02115

Contributed by George B. Benedek, November 1, 2001

Increasing evidence supports the hypothesis that amyloid β-protein (Aβ) assembly is a key pathogenic feature of Alzheimer's disease. Thus, understanding the assembly process offers opportunities for the development of strategies for treating this devastating disease. In prior studies, Aβ was found to form micelle-like aggregates under acidic conditions. These structures exhibited an average observed hydrodynamic radius of 7 nm. They were found to be in rapid equilibrium with Aβ monomers or low molecular weight oligomers, and were centers of fibril nucleation. Here the technique of small angle neutron scattering has been used to determine the structure of these Aβ micelles. The data reveal that the micellar assemblies comprise 30–50 Aβ monomers and have elongated geometries. The best fit of the data to a uniform spherocylinder yields a radius ≈2.4 nm and cylinder length ≈11 nm. These structure parameters remain constant over more than a decade in concentration range. The concentration independence of the length of the cylindrical aggregate indicates the presence of an internal nonrepetitive structure that spans the entire length of the Aβ assembly.

Alzheimer's disease (AD) is a progressive neurodegenerative disorder characterized in part by extensive amyloid deposition in the brain parenchyma and vasculature (1). These amyloid deposits are formed by the amyloid β-protein (Aβ), a proteolytic fragment of the larger amyloid β-protein precursor (AβPP) (2). Compelling data support the hypothesis that Aβ production and fibril assembly are linked to AD (3). For example, mutations in gene encoding AβPP, or in genes encoding proteins involved in the Aβ metabolism, are associated with familial forms of AD or of cerebral amyloid angiopathy. In all cases thus far studied, these mutations increase Aβ production, increase the relative amount of the particularly amyloidogenic 42-residue form of Aβ, or alter the biophysical properties of the mutant Aβ peptide facilitating its self-association or retarding its catabolism. Recent studies in humans, in transgenic mice, and *in vitro*, suggest that important effectors of Aβ-mediated neuronal injury and death may be small oligomeric assemblies of Aβ (4). Understanding the earliest phases of Aβ fibril formation, in particular oligomerization and other prenucleation interactions, is thus of great importance for identifying potential therapeutic targets.

Previously (5), quasielastic light scattering (QLS) spectroscopy was used to monitor the kinetic evolution of the size distribution of Aβ(1–40) assemblies formed under acidic conditions. These experiments showed that above a critical concentration $c^* \approx 0.1$ mM, Aβ formed micelle-like structures with an average observed hydrodynamic radius $R_h \approx 7$ nm. These micelles[‖] formed immediately on dissolution of the protein and were in equilibrium with low molecular weight, possibly monomeric, components of the Aβ solution. Analysis of the temporal evolution of the fibril length distribution at different total Aβ concentrations revealed that micelles are centers of fibril nucleation (6). This conclusion explained the observed concentration independence of the final fibril size and the fibril growth rate at total Aβ concentrations exceeding c^*, the critical concentration.

The ability of the Aβ micelles formed at low pH to control Aβ fibril nucleation makes their structure of particular interest. One method to elucidate the details of this structure is small angle neutron scattering (SANS). SANS experiments can provide useful information regarding the aggregation number, shape, and dimensions of the structure in question. Previous studies (7, 8) have demonstrated the feasibility of SANS measurements on fibrillar Aβ(10–35) in D_2O. Using quasielastic light scattering spectroscopy, we found that in 0.1 N DCl in D_2O the kinetics of Aβ(1–40) fibrillization is very similar to that observed in HCl/H_2O solution. Importantly, in the deuterated environment, as in water, particles with hydrodynamic radius $R_h \approx 7$ nm were found above the critical concentration. We report here the results of SANS studies of the structure of Aβ micelles formed in 0.1 N DCl/D_2O and the effects of Aβ concentration on this structure.

Materials and Methods

Sample Preparation. Aβ(1–40) was synthesized on an automated peptide synthesizer (Applied Biosystems, Model 430A) by using fluorenylmethoxycarbonyl (Fmoc) chemistry, as described (9). All samples were prepared by diluting the lyophilized peptide into 0.1 N DCl in D_2O. Two sets of experiments were performed. In the first set, samples of Aβ at concentrations of 2.2 mg/ml and 5.0 mg/ml were centrifuged at $10^4 \times g$ for 10 min to remove preexisting aggregates. For the second set of experiments, samples were filtered through a 20-nm inorganic membrane filter (Anatop 10 plus, Whatman) to final concentrations of 0.60, 0.40, 0.31, 0.27, 0.22, and 0.05 mg/ml as determined by quantitative amino acid analysis (AAA) following the SANS experiments. Aliquots of each sample also were taken for QLS. The aliquot for SANS was frozen immediately at −80°C and transported to the reactor at −20°C.

Quasielastic Light Scattering. QLS experiments were performed with a 144-channel Langley-Ford model 1097 correlator (Langley-Ford, Amherst, MA) and a Coherent Innova 90 argon laser (514 nm; Coherent Radiation, Santa Clara, CA). The scattering angle was 90°. The sample holder temperature was controlled using an Endocal water bath (Neslab Instruments, Portsmouth, NH). The measured correlation functions were analyzed as

Abbreviations: Aβ, amyloid β-protein; SANS, small angle neutron scattering; QLS, quasielastic light scattering.

[¶]To whom reprint requests should be addressed at: Room 13-2005, Massachusetts Institute of Technology, 77 Massachusetts Avenue, Cambridge, MA 02139-4307. E-mail: gbb@mit.edu.

[‖]The term "micelle(s)" is used herein for convenience in order to describe an oligomeric Aβ assembly with physicochemical and structural properties consistent with those of well characterized micelle-forming substances.

The publication costs of this article were defrayed in part by page charge payment. This article must therefore be hereby marked "*advertisement*" in accordance with 18 U.S.C. §1734 solely to indicate this fact.

 www.pnas.org/cgi/doi/10.1073/pnas.012584899

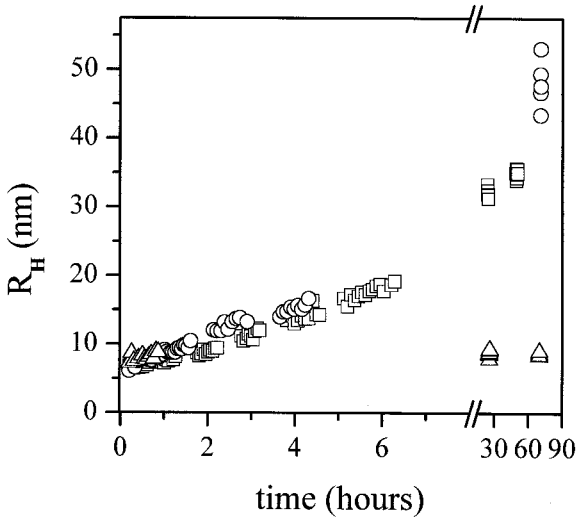

Fig. 1. Time evolution of the apparent hydrodynamic radius of Aβ aggregates, obtained by QLS, at concentration 0.40 mg/ml. The solvents are 0.1 N HCl in H_2O at 25°C (□); 0.1 N DCl in D_2O at 25°C (○); 0.1 N DCl in D_2O at 4°C (△).

described by Thomas *et al.* (10). QLS experiments confirm that the course of fibrillogenesis in DCl/D_2O (used for SANS measurements) at 25°C was very similar to that observed in HCl/H_2O, though slightly slower. Furthermore, it was shown that freezing and thawing of Aβ dissolved in 0.1 N DCl/D_2O, as in 0.1 N HCl/H_2O (11), did not alter the course of fibrillogenesis. SANS experiments require several hours, more than the duration of the initial lag phase of the fibrillogenesis process at room temperature. Fortunately, the rate of fibril growth slows dramatically at lower temperatures (11). To evaluate the feasibility of SANS studies of micelle structure, QLS experiments were carried out at 4°C in 0.1 N DCl/D_2O at an Aβ concentration c_0 = 0.4 mg/ml. These experiments showed that the light scattering is dominated for at least 70 h by particles of $R_h \approx 7$ nm (Fig. 1). Additional QLS experiments were conducted on aliquots taken from samples prepared for SANS measurements to verify the particle size distribution of these samples.

SANS. SANS experiments were conducted at National Institute of Standards and Technology, Center for Neutron Research, Gaithersburg, MD. The 40-m SANS station was used with an incident wavelength $\lambda = 5$ Å with a spread $\Delta\lambda/\lambda = 11\%$. The neutron source to sample distance was 13.12 m. All measurements were 1 h long. Samples from the first set, with nominal concentrations of 2.2 mg/ml and 5.0 mg/ml, were measured twice, at 4°C and then at 10.9°C. A Helma cuvette of 2 mm thickness and circular side 25 mm in diameter was used. At each temperature, the measurements were done at two different sample-to-detector distances. One provides magnitudes of the Q-vector in the range 0.0054–0.04 Å^{-1} (sample-to-detector distance of 10 m) and the other from 0.011–0.28 Å^{-1} (sample-to-detector distance of 2 m). Low Q range measurements were made first. In the second set of experiments, six samples with concentrations from 0.05–0.60 mg/ml were measured at 4°C, in high Q range only. A Helma cuvette of 5 mm thickness and 19 mm diameter was used. The actual concentrations of these samples were determined *a posteriori* by AAA and were found to be 0.60, 0.40, 0.31, 0.27, 0.22, and 0.05 mg/ml.

SANS data analysis. Data of SANS are presented in terms of $I(Q)$, the differential scattering cross section per unit volume, which is the probability for a neutron to be scattered into a unit solid angle per unit path length. $I(Q)$ is measured in cm^{-1} and depends on Q, the scattering (Bragg) wave vector,

$$Q = \frac{4\pi \sin(\theta/2)}{\lambda}. \quad [1]$$

Here λ is the wavelength of the neutrons and θ is the scattering angle. For a monodisperse solution, $I(Q)$ is given by (12)

$$I(Q) = I_0 \bar{P}(Q) S(Q). \quad [2]$$

Here $\bar{P}(Q)$, the normalized structure factor, accounts for the shape of the scattering particle, and $S(Q)$, the interparticle structure factor, accounts for the correlation between the position of micelles due to interaction. The forward cross section I_0 is given by

$$I_0 = N_A m_o^2 c_m (b_m - \rho_s v_m)^2 \times 10^3, \quad [3]$$

where c_m is the molar concentration of micelles (mol/l), m_o is the number of Aβ monomers in a single micelle, and N_A is Avogadro's number. The contrast, $b_m - \rho_s v_m$, measured in centimeters, accounts for the difference of neutron scattering power between Aβ and that of the solvent (D_2O in this case). The contrast depends on the scattering length density of D_2O, $\rho_s = 6.34 \times 10^{10}$ cm^{-2}, on the sum of the scattering lengths of all the amino acids in the peptide, b_m, and on the sum of the dry volumes of each amino acid, v_m. We calculated parameters b_m and v_m by using values provided by Jacrot and Zaccai (13). Assuming that all labile hydrogens undergo hydrogen/deuterium (H/D) exchange, $b_m - \rho_s v_m = -1.81 \times 10^{-10}$ cm; assuming no H/D exchange, $b_m - \rho_s v_m = -2.43 \times 10^{-10}$ cm.

In a dilute solution, when correlations between particles can be neglected, $S(Q) = 1$. The angular dependence of the neutron scattering is then determined by the particle structure factor $\bar{P}(Q)$, which depends on the size and shape of the scattering particle (12). The experimentally observed intensity of neutron scattering decreases with angle much slower than expected for spherical scatterers, clearly showing that our samples contained elongated objects. Many reasonable models, such as the ellipsoid, the cylinder, or the spherocylinder, could fit our data equally well. The overall features of the object (length, aspect ratio, and mass) do not depend on the model used to fit the data in any significant way. We chose here the spherocylindrical model (cylinder of length L with hemispherical end caps of radius R) and used MATLAB (Mathworks, Natick, MA) software to numerically calculate values of spherocylinders' structure factor within the data fitting procedure.

Determination of aggregation number m_o and critical concentration c^*. In previous work (5, 11), a monomer–micelle equilibrium was postulated to exist at the initial stage of Aβ(1–40) fibrillogenesis. Let the solution of Aβ have a molar concentration c_m of micelles and a molar concentration c_1 of monomers. The total molar concentration (c_0) of Aβ is then

$$c_0 = c_1 + m_o c_m. \quad [4]$$

For simplicity we assume that all micelles have the same aggregation number m_o and the same structure. In this simple two-state model, the concentration of micelles is proportional to $c_1^{m_o}$ and can be written as (11)

$$c_0 - c_1 = m_o c_m = c^* \left(\frac{c_1}{c^*}\right)^{m_o}. \quad [5]$$

Eq. **5** introduces the critical micellar concentration c^*. According to Eq. **4**, c_1 in Eq. **5** can be replaced by $c_o - m_o c_m$ producing an equation

$$\frac{m_o c_m}{c^*} = \left(\frac{c_o - m_o c_m}{c^*}\right)^{m_o} \quad [6]$$

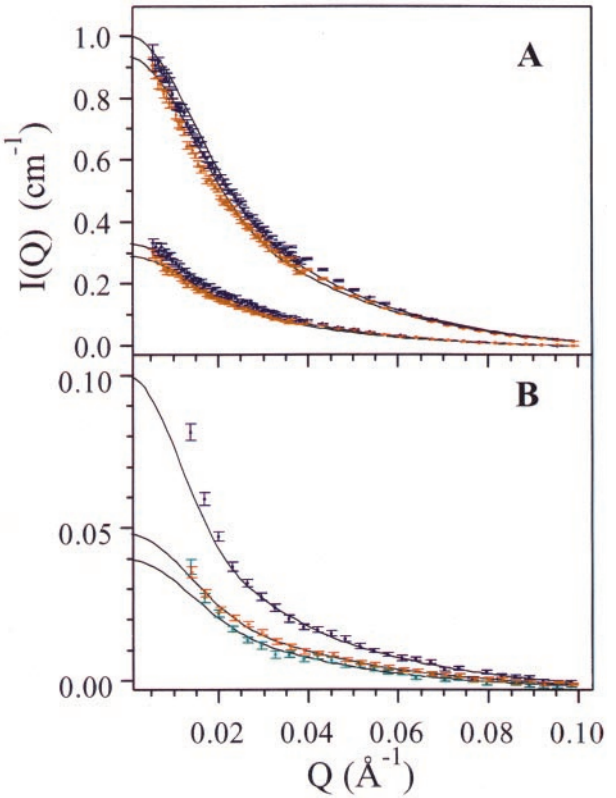

Fig. 2. Differential cross section per unit volume of neutron scattering $I(Q)$ versus magnitude of the scattering vector Q. (*A*) c_0 = 5.0 mg/ml (top data points) and 2.2 mg/ml (bottom data points). The solid lines correspond to the theoretical fit for a spherocylinder. Data at 10.9°C (blue) and at 4°C (red) are fitted separately. (*B*) $I(Q)$ for the second set of samples with lower concentrations: blue, c_0 = 0.60 mg/ml; red, c_0 = 0.40 mg/ml; green, c_0 = 0.31 mg/ml. The solid lines are the theoretical fits with the parameters listed in Table 1.

that implicitly expresses c_m as a function of c_0 and two parameters: the aggregation number m_0 and the critical concentration c^*. By calculating c_m from Eq. **6** and substituting the result into Eq. **3**, we can obtain the dependence of I_0 on c_0 for any parameters c^* and m_o. We then can determine the values of the parameters that best fit the experimentally observed concentration dependence of neutron scattering intensity.

Results and Discussion

In Fig. 1 we compare the fibrillogenesis in solutions of 0.40 mg/ml of Aβ(1–40) in 0.1 N DCl/D_2O at 25°C and 4°C and in 0.1 N HCL/H_2O at 25°C. This figure shows that the initial size of the aggregates present in solution is approximately 7 nm in all three cases. The initial rate of fibril growth observed at 25°C is similar in both solutions, although fibers seem to grow slightly faster in D_2O. After approximately 2 days, fibrils reach their final size, which is bigger in the case of D_2O. This greater size may result from a slightly faster elongation rate, a slower nucleation rate, and fewer preexisting seeds in the D_2O sample (6). The data in Fig. 1, obtained by QLS, suggests that the micelle-like aggregates formed at low pH immediately on dissolving Aβ in heavy water are the same as those formed in H_2O. At 4°C, the rate of fibril growth slows dramatically (11). Indeed, in 0.1 N DCl/D_2O at 4°C no aggregation occurs for at least 70 hours. This provides a window of time sufficient for SANS experiments.

The results of SANS experiments are summarized in Fig. 2. This figure shows the differential cross section of neutron scattering $I(Q)$ of Aβ samples in a Q range from 0.0054–0.1 Å^{-1}. The data obtained in the first set of experiments for the samples

Table 1. Summary of the micelle dimensions at each C_0 value

c_0, mg/ml	R, nm	L, nm	I_0^a	I_0^b
5.0	2.3 ± 0.1	11.1 ± 0.3	0.926	0.927
2.2	2.3 ± 0.1	10.5 ± 0.4	0.279	0.289
0.6	2.5 ± 1.2	13.9 ± 7.0	0.102	0.084
0.40	2.4 ± 0.1	11.5 ± 1.2	0.050	0.049
0.31	2.5 ± 0.2	11.4 ± 3.9	0.044	0.042

Parameters R and L are the dimension of the spherocylinder obtained from the fit of individual data, I_0^a being the corresponding intensity of forward scattering. Parameter I_0^b is the intensity of forward scattering that provides the best fit for fixed R = 2.4 nm and L = 11.0 nm.

with concentrations c_0 of 5.0 mg/ml and 2.2 mg/ml are shown in Fig. 2*A*. We see that in both samples the shape of $I(Q)$ at 4°C (red) is the same as that at 10.9°C (blue). Thus, the particle structure factor of the micelles is independent of temperature. However, at 10.9°C, $I(Q)$ values are slightly higher than that at 4°C. This increase of scattering intensity is probably a consequence of aggregation or fibril formation in the samples. Indeed, measurements at 10.9°C were conducted after measurements at 4°C and samples were subjected to an additional freeze–thaw cycle. Fig. 2*B* presents results for the second set of samples. These measurements were taken at 4°C at high Q range only. The data for samples with concentrations of 0.60 mg/ml, 0.40 mg/ml, and 0.31 mg/ml are shown. At lower concentrations, the SANS scattering intensity was too weak to produce meaningful structural information.

Solid lines in Fig. 2 are the best theoretical fits to a spherocylindrical model determined individually for each concentration and temperature. In the fitting procedure we have assumed that all scatterers have the same size and shape. As is shown in Fig. 2 our data are consistent with this assumption in the region $Q > 0.025$ Å^{-1} for all concentrations studied. We believe that the deviations shown in Fig. 2 for $Q < 0.025$ Å^{-1} are produced by large aggregates or fibrils. Indeed, the existence of such aggregates was confirmed in control QLS measurements. Alternatively, one could invoke polydispersity in the micelle distribution to better fit the low Q scattering data. However, thermodynamic consideration shows that, in the case of a significantly polydisperse distribution, an increase in concentration should shift the equilibrium in favor of larger micelles, resulting in an increase in the mean size. This increase is not borne out by the data.

The parameters of the spherocylinders, R and L, as well as the intensity of forward scattering, I_0^a, used in fits of the 4°C data, are listed in Table 1. It is clear from Table 1 that the radii of the putative spherocylindrical micelles are the same at all concentrations, within the experimental error of measurements. The parameter L also shows no systematic concentration dependence. We believe that the variation of the parameters R and L observed in Table 1 is due to the presence of aggregates or fibrils and not to the actual changes in micelle dimensions—i.e., in all of our samples particles of the same size are responsible for neutron scattering. This being the case, the normalized background-corrected neutron scattering intensity $\bar{P}(Q)$ is the same and only the magnitudes I_0 vary in proportion to the micelle concentration (c_m). Indeed, on a logarithmic scale, data curves representing scattering at different concentrations are parallel to each other (Fig. 3). Note that the slow, nearly linear decrease of $\log I(Q)$ in a significant range of Q values above 0.03 Å^{-1} indicates scattering from elongated structures. Solid lines in Fig. 3 represent the best fit of the entire set of SANS data assuming scattering from the same uniform spherocylindrical particles with R = 2.4 nm and L = 11 nm. Keeping these parameters fixed, we determined the cross section of forward scattering for every individual measurement, I_0^b. As seen in Table 1, the

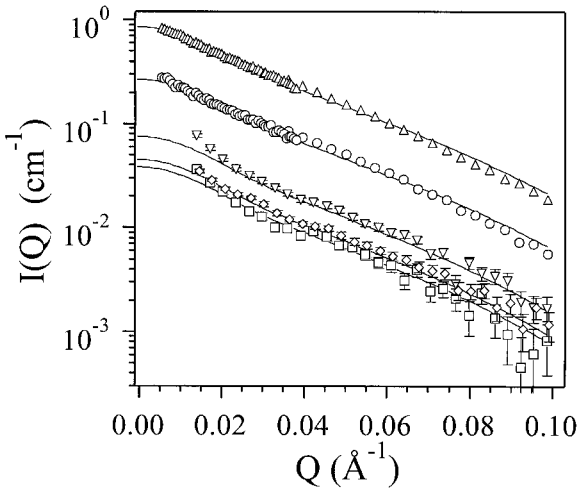

Fig. 3. The same experimental data as in Fig. 2, shown in logarithmic scale. The solid lines are calculated for a spherocylinder with dimensions $R = 2.4$ nm and $L = 11.0$ nm and I_0^b listed in Table 1. All data shown were taken at 4°C. Two topmost curves correspond to samples of 5.0 mg/ml (△) and 2.2 mg/ml (○) both at high and low Q range. The rest of the measurements, low Q range only, are: $c_0 = 0.60$ mg/ml (▽); $c_0 = 0.40$ mg/ml (◇, offset slightly to the right for clarity); and $c_0 = 0.31$ mg/ml (□).

difference between I_0^b, deduced with the assumption that the size and shape of micelles remains fixed at all concentrations, and I_0^a, obtained without this assumption, is within the experimental uncertainty. Thus, above the critical micelle concentration, our experiments show no concentration dependency in the size and shape of Aβ micelles.

Having determined the structural parameters of micelles, we now turn to an analysis of the concentration dependence of the intensity of neutron scattering. From this we can find parameters m_0 and c^* that best fit the experimental $I_0(c_0)$. In Fig. 4 we show with filled squares (■) the forward cross sections of neutron scattering I_0^b at various Aβ concentrations. In addition to data from Table 1 (only the three lowest concentrations are shown), we present forward cross sections for concentrations of 0.05 mg/ml and 0.27 mg/ml. Although at these concentrations the intensity of scattering is too low to give reliable structural

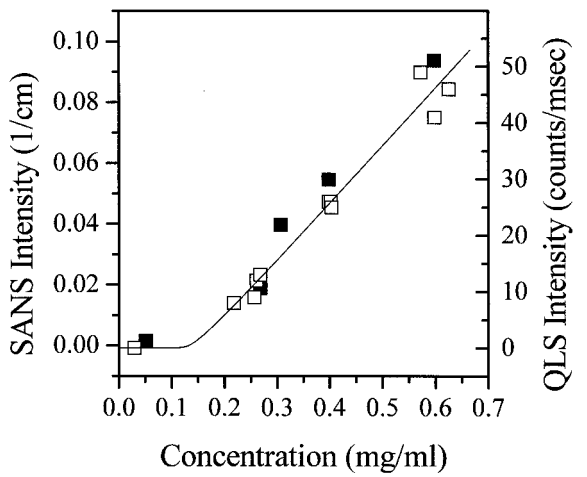

Fig. 4. SANS and QLS scattering intensities as functions of concentration at 4°C. (■, SANS forward cross section I_0^b; □, QLS intensity normalized so as to overlay with SANS data. The solid line represents the theoretical prediction for $c^* = 0.15$ mg/ml and $m_0 = 29$.

information, the overall scattering cross section can be determined. At the lowest concentration of 0.05 mg/ml, no scattering from micelles is observed. In effect, this sample provides the background neutron scattering intensity. The solid line in Fig. 4 shows the dependence of I_0 on the total concentration c_0 predicted by Eqs. **3** and **6**. Open squares (□) represent the relative QLS intensity of light scattered at 90°, scaled to overlay the SANS data. Both SANS and QLS data agree with each other and are well described by the theoretical curve.

The physical interpretation of the data presented in Fig. 4 is as follows. For $c_0 < c^*$, Eq. **5** shows that $c_1 < c^*$ and $m_0 c_m \cong 0$—i.e., very few micelles are present, and $c_0 \cong c_1$. On the other hand, for $c_0 > c^*$, $c_1 \equiv c^*$ will satisfy Eq. **5** for all c_0. Hence $m_0 c_m \cong c_0 - c^*$. Thus for $c_0 > c^*$ the dependence of I_0 versus c_0 is represented by a line with x intercept of c^* and with a slope of $N_A m_0^2 (b_m - \rho_s v_m)^2 \times 10^3 = 5.74 \times 10^{10}$ cm^2. It should be noted that the critical micellar concentration observed in the present work, $c^* = 0.15$ mg/ml, is about one-third of that reported previously by Lomakin *et al.* (5). This discrepancy arises because the nominal peptide concentrations in the earlier study were determined by dissolving lyophilized peptide to a desired concentration without controlling the effects of insoluble aggregated material or adventitiously bound nonpeptide material. In contrast, in the present work the concentration of the protein was determined by amino acid analysis (AAA) after filtration through 20-nm filters in order to remove preexisting fibrils and aggregates.

From the observed slope we can calculate the value m_0 if the contrast value $b_m - \rho_s v_m$ is known. Using the contrast -1.81×10^{-10} cm obtained by assuming that all labile hydrogen atoms in Aβ are exchanged by deuterium, we obtain $m_0 = 54$. Kheterpal *et al.* (14) have shown that in monomeric Aβ(1–40) such an exchange indeed takes place, whereas in fibrillar Aβ(1–40) only about 50% of the labile hydrogen undergo H/D exchange. Furthermore, evidence provided by Rene *et al.* (15) indicates that under acidic conditions certain amino groups undergo slow H/D exchange relative to the duration of our experiments. We therefore do not know accurately the level of H/D exchange. However, both the fact that Aβ forms micelle-like aggregates in which hydrophobic regions are less accessible to solvent, and that acidic (0.1 N DCl) conditions were used, should reduce the number of labile hydrogen atoms that were actually replaced by deuterium during the experiments. Thus, the actual contrast is higher than the value used above and $m_0 = 54$ is therefore an overestimation of the actual aggregation number. A lower limit on m_0 can be obtained if we incorporate a maximum contrast value of -2.43×10^{-10} cm corresponding to no H/D exchange. The slope of the data in Fig. 4 then yields a value $m_0 = 29$. Note that previously (5) an estimate $15 < m_0 < 70$ had been reported and that $m_0 = 25$ had been chosen for analysis.

The volume of a spherocylinder with $R = 2.4$ nm and $L = 11$ nm is 257 nm^3. For $m_0 = 29$ (in the absence of H/D exchange), this corresponds to 8.8 nm^3/monomer. For Aβ monomer with a molecular weight 4,330 this value implies a dry density of 0.8 g/cm^3, which is more than we would expect for hydrated protein. If all labile H atoms undergo H/D exchange ($m_0 = 54$), the apparent density becomes even higher, 1.5 g/cm^3. This value suggests that our model of a uniform spherocylinder underestimates the actual particle size. In reality, H/D exchange occurs mostly on the surface of micelle-like aggregates where hydrophilic groups are concentrated. Consequently, the contrast of the outer layer of these micelles is reduced and the value of $R = 2.4$ nm probably reflects the radius of the hydrophobic core of the micelle rather than its geometrical radius. Also, the hydrodynamic radius of a spherocylinder [calculated using expressions provided by de la Torre and Bloomfield (16)] with dimensions of $R = 2.4$ nm and $L = 11$ nm is $R_h = 4.7$ nm. This value is less than the R_h observed in QLS experiments, which is typically ≈7

nm (Fig. 1). However, it should be noted that a few large fibers formed in solution can significantly increase the average R_h observed in QLS experiments ($Q = 0.00325$ Å^{-1}) in which particles up to ≈30 nm in radius contribute to the scattering proportional to their mass squared. These fibers are practically unobserved in SANS measurements because, in the Q range above 0.025 Å^{-1}, particles larger than ≈10 nm scatter only proportional to their mass. It is clear that the SANS and the QLS methods probe different features of the particles. The value of $R_h = 4.7$ nm likely provides the lower limit for the actual R_h.

The fact that the Aβ micelle-like intermediates in our experiments are elongated objects that do not change size with Aβ concentration has important consequences. Elongated, worm-like micelles are well known (10, 17). However, the length of those micelles increases with concentration. Indeed, if the object is built from repetitive units arrayed in one dimension, it therefore can be of any length and if this object is in equilibrium with monomers, then an increase in concentration should lead to an increase in the average aggregation number, according to Le Chatelier's principle. No increase in the size of the Aβ micelles was observed in the SANS experiment over greater than a decade of concentration variation nor was any concentration dependence of the hydrodynamic radius seen in previous QLS measurements (5, 11). At the same time, compelling evidence indicates that Aβ micelles are in equilibrium with monomers and/or oligomers. Furthermore, our SANS data clearly indicate an assembly with an elongated structure. We therefore conclude that these micellar structures differ significantly from classical cylindrical micelles in that they are not built from repetitive units. One potential model of the structure of the spherocylindrical Aβ micelle is shown schematically in Fig. 5. In this model the micelle is an elongated cylindrical object in which Aβ monomers are stretched along the cylinder axis.

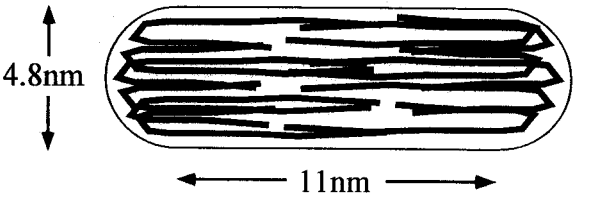

Fig. 5. Schematic model of Aβ assembly consistent with SANS data.

Our SANS experiments confirmed that upon dissolution under acidic condition in concentration above $c^* = 0.15$ mg/ml, Aβ monomers form micelle-like aggregates consisting of about 30 monomers. These aggregates are of elongated shape with a particle structure factor that is well described by a uniform spherocylinder with a radius of $R = 2.4$ nm and a length of the cylindrical part of $L = 11$ nm. The size and the shape of the aggregate remains the same over a decade of concentrations.

We are grateful to Ms. Margaret Condron for expert technical assistance. We are grateful to the National Institute of Standards and Technology, Center for Neutron Research for providing SANS beam time for this research. This work was supported by National Institutes of Health Grant 1PO1AG14366 (to G.B.B. and D.B.T.) and by the Foundation for Neurologic Diseases (D.B.T.). The work of S.H.C. was supported by a grant from Materials Chemistry Program of the U.S. Department of Energy.

1. Selkoe, D. J. (1991) *Neuron* **6,** 487–498.
2. Selkoe, D. J. (1999) *Nature (London)* **399,** A23–A31.
3. Hardy, J. (1997) *Proc. Natl. Acad. Sci. USA* **94,** 2095–2097.
4. Klein, W. L., Krafft, G. A. & Finch, C. E. (2001) *Trends Neurosci.* **24,** 219–224.
5. Lomakin, A., Chung, D. S., Benedek, G. B., Kirschner, D. A. & Teplow, D. B. (1996) *Proc. Natl. Acad. Sci. USA* **93,** 1125–1129.
6. Lomakin, A., Teplow, D. B., Kirschner, D. A. & Benedek, G. B. (1997) *Proc. Natl. Acad. Sci. USA* **94,** 7942–7947.
7. Thiyagarajan, P., Burkoth, T. S., Urban, V., Seifert, S., Benzinger, T. L. S., Morgan, D. M., Gordon, D., Meredith, S. C. & Lynn, D. G. (2000) *J. Appl. Crystallogr.* **33,** 535–539.
8. Burkoth, T. S., Benzinger, T. L. S., Urban, V., Morgan, D. M., Gregory, D. M., Thiyagarajan, P., Botto, R. E., Meredith, S. C. & Lynn, D. G. (2000) *J. Am. Chem. Soc.* **122,** 7883–7889.
9. Walsh, D. M., Lomakin, A., Benedek, G. B., Condron, M. & Teplow, D. B. (1997) *J. Biol. Chem.* **272,** 22364–22372.
10. Thomas, H. G., Lomakin, A., Blankschtein, D. & Benedek, G. B. (1997) *Langmuir* **13,** 209–218.
11. Kusumoto, Y., Lomakin, A., Teplow, D. B. & Benedek, G. B. (1998) *Proc. Natl. Acad. Sci. USA* **95,** 12277–12282.
12. Chen, S.-H. (1986) *Annu. Rev. Phys. Chem.* **37,** 351–399.
13. Jacrot, B. & Zaccai, G. (1981) *Biopolymers* **20,** 2413–2426.
14. Kheterpal, I., Zhou, S., Cook, K. D. & Wetzel, R. (2000) *Proc. Natl. Acad. Sci. USA* **97,** 13597–13601. (First Published November 21, 2000; 10.1073/pnas.250288897)
15. Rene, R., Sehr, P., Wagner, G. & Wurthrich, K. (1979) *J. Mol. Biol.* **130,** 19–30.
16. de la Torre, J. G. & Bloomfield, V. A. (1981) *Q. Rev. Biophys.* **14,** 81–139.
17. Blankstein, D., Thurston, G. & Benedek, G. B. (1986) *J. Phys. Chem.* **85,** 7268–7288.